

Combined Effect of Heating Rate and Microalloying Elements on Recrystallization During Annealing of Dual-Phase Steels



MARION BELLAVOINE, MYRIAM DUMONT, JOSÉE DRILLET,
VÉRONIQUE HÉBERT, and PHILIPPE MAUGIS

Adjusting ferrite recrystallization kinetics during annealing is a way to control the final microstructure and thus the mechanical properties of advanced cold-rolled high-strength steels. Two strategies are commonly used for this purpose: adjusting heating rates and/or adding microalloying elements. The present work investigates the effect of heating rate and microalloying elements Ti, Nb, and Mo on recrystallization kinetics during annealing in various cold-rolled Dual-Phase steel grades. The use of combined experimental and modeling approaches allows a deeper understanding of the separate influence of heating rate and the addition of microalloying elements. The comparative effect of Ti, Nb, and Mo as solute elements and as precipitates on ferrite recrystallization is also clarified. It is shown that solute drag has the largest delaying effect on recrystallization in the present case and that the order of solute drag effectiveness of microalloying elements is $Nb > Mo > Ti$.

<https://doi.org/10.1007/s11661-018-4642-z>

© The Minerals, Metals & Materials Society and ASM International 2018

I. INTRODUCTION

DUAL-PHASE (DP) steels are the most developed and widely used advanced high-strength steels.

Their final microstructure is made of a hard martensitic phase dispersed in a soft bainitic/ferritic matrix and offers a good compromise between high strength and high formability.^[1-3] The processing route for cold-rolled DP products consists of hot-rolling followed by cold-rolling and continuous annealing. Continuous annealing of cold-rolled sheets consists of heating and soaking in the intercritical temperature range, leading to the formation of a microstructure composed of ferrite and austenite. Subsequent cooling leads to the final microstructure made of martensite, bainite, and ferrite. As the microstructure obtained at the end of the intercritical annealing has a major influence on the final mechanical properties of DP steels, understanding microstructural changes during this stage is of

considerable interest. These microstructural changes are the results of three major mechanisms: precipitation of microalloying elements, ferrite recrystallization, and austenite formation. These mechanisms may occur simultaneously or successively and may interact with each other. Their kinetics and interactions essentially depend on three key factors: the nominal composition of the steel, the microstructure after cold-rolling, and the processing parameters of the annealing cycle (heating rate, soaking temperature, and soaking time). Monitoring the microstructure obtained at the end of annealing thus implies to know and to take benefit of the separate role of these factors on the different mechanisms.

Recrystallization is one of the mechanisms that are essential to control. Recrystallization is the formation of new dislocation-free grains within the deformed structure by the migration of high-angle grain boundaries.^[4] Recrystallization kinetics are important to control for two main reasons. The first reason is that recrystallization and subsequent grain growth determine the final ferrite grain size. The second reason is that recrystallization strongly affects austenite formation and distribution, and thus the morphology of the microstructure.^[6,7] In particular, it was shown that the overlap of ferrite recrystallization and austenite formation results in a finer, more heterogeneous and anisotropic microstructure.^[7] The cold-rolled microstructure influences recrystallization kinetics during annealing through the amount of the stored energy of deformation. It is indeed well known that the stored energy is the driving force for

MARION BELLAVOINE is with the IM2NP – UMR CNRS 7334 – Aix-Marseille Université, Univ. Toulon, Faculté des Sciences et Techniques de St-Jérôme – Service 251, 13 397, Marseille Cedex 20, France and also with ArcelorMittal Research SA, Maizières-les-Metz, France. MYRIAM DUMONT and PHILIPPE MAUGIS are with the IM2NP – UMR CNRS 7334 – Aix-Marseille Université, Univ. Toulon, Faculté des Sciences et Techniques de St-Jérôme – Service 251. Contact e-mail: myriam.dumont@univ-amu.fr JOSÉE DRILLET and VÉRONIQUE HÉBERT are with ArcelorMittal Research SA.

Manuscript submitted September 19, 2017.

Article published online May 4, 2018

recrystallization in deformed specimens.^[4] To control recrystallization kinetics for a given cold-rolled microstructure, two main strategies can be used: adjusting heating rates and/or adjusting the content of microalloying elements delaying recrystallization. The effect of heating rate on ferrite recrystallization kinetics is well established^[6,8,9]: an increase in heating rate retards recrystallization and increases the temperature of complete recrystallization. While the effect of microalloying elements on impeding austenite recrystallization during hot rolling has been extensively studied,^[10–12] their effect on impeding ferrite recrystallization during annealing of cold-rolled steels has been more scarcely investigated.^[13,14] Two main questions arise regarding the effect of microalloying elements: the first one deals with the comparative effectiveness of microalloying elements as solute elements and as precipitates. Indeed, the microalloying elements still available in supersaturated solution in the cold-rolled sheet precipitate as fine (Ti,Nb,Mo)(C,N) particles during the annealing treatment. Microalloying elements can thus affect recrystallization by two mechanisms: either by solute drag as solute elements^[15,16] and/or by Zener-pinning on grain boundaries as precipitates.^[17] The comparative effectiveness of solute and precipitates on delaying recrystallization is not always clearly established. Experimental investigations require determining the precipitation state to be able to compare the driving force for recrystallization to the Zener pinning force exerted by precipitates. There has been a long-lasting debate about this topic in austenite, some studies reporting either Zener pinning^[18] or solute drag^[19] as the dominant effect, or a contribution of both effects.^[12,20] The topic has been more scarcely addressed in ferrite. Using a theoretical approach, Hutchinson *et al.*^[21] concluded that under most cases, Nb atoms in solution are more effective in ferrite, whereas NbC precipitates are usually more effective in austenite. The second question deals with the comparative effectiveness of the different microalloying elements (Ti, Nb, and Mo) on retarding recrystallization. This question requires addressing the effect of microalloying elements on carbonitride precipitation on the one hand, and their separate solute drag effect on the other hand. Previous studies regarding austenite recrystallization showed that Nb has the strongest solute drag effect followed by Mo, and that Ti and V have the smallest solute effect.^[12,20,22]

In order to bring some clarifications regarding these effects in the case of ferrite recrystallization, we investigate both precipitation and ferrite recrystallization depending on the heating rate during annealing of various cold-rolled dual-phase steel grades.

II. MATERIALS AND EXPERIMENTAL PROCEDURE

Five steel grades have been studied (Table I). The nominal chemical compositions were defined in order to investigate the effect of a change of microalloying element content for a similar cold-rolled microstructure.

Cold-rolled sheets were obtained by hot rolling of laboratory ingots followed by 50 pct cold-rolled reduction. Cold-rolled specimens with a thickness of 1.25 mm were annealed using heating rates of either 1 or 10 K/s. Continuous heating was performed using either an annealing simulator or a DT 1000 thermal simulator and interrupted at different temperatures by water quenching and helium blowing respectively. In both cases, the cooling rate was larger than 300 K/s so that all the austenite transformed into martensite during cooling. The annealing simulator furnace was used to anneal samples for gravimetric analysis of electrolytic extraction residues on 10 cm² areas to obtain the amount of precipitated Nb, Ti, and Mo. Smaller samples (length of 12 mm and section of 3 × 1.25 mm²) dedicated to field electron gun scanning electron microscopy (FEG-SEM) and transmission electron microscopy (TEM) analysis were annealed using DT 1000 thermal simulator.

Microstructures of annealed samples were observed by FEG-SEM JEOL[®] JSM-7800F at a quarter of the sheet thickness in the RD–ND plane (Rolling Direction–Normal Direction to the sheet surface). Samples were prepared by standard metallographic techniques followed by Dino etching (140 ml of distilled water, 100 ml of H₂O₂, 4 g of oxalic acid, 2 ml of H₂SO₄, and 1.5 ml of HF). Phase fractions were determined by manual phase identification and image analysis of FEG-SEM images. Dino etching makes non-recrystallized ferrite grains to appear as elongated with surface irregularities while recrystallized ferrite grains appear as polygonal with a smooth surface. Dino etching also allows the identification of martensite thanks to the stronger etching of this phase compared to ferrite together with its typical serrated aspect.

Table I. Nominal Chemical Composition of the Five Grades Under Investigation

Weight Percent	C	Mn	Cr + Si	Nb	Ti	Mo	N	B
Steel A (Ref)	0.075	2.5	0.6	0.028	0.027	—	0.004	0.002
Steel B (Ref + Nb)	0.075	2.5	0.6	0.047	0.026	—	0.004	0.002
Steel C (Ref + Ti)	0.075	2.5	0.6	0.027	0.040	—	0.004	0.002
Steel D (Ref + Nb + Ti)	0.075	2.5	0.6	0.044	0.040	—	0.004	0.002
Steel E (Ref + Mo)	0.075	2.5	0.6	0.025	0.029	0.090	0.005	0.002

Precipitation state was characterized using scanning transmission electron microscopy (STEM)-Bright Field (BF) analysis on electro-thinned foils. These were performed on Jeol® JEM 2100F at 200 kV. Image analysis of STEM-BF images combined with local thickness measurements carried out through electron energy-loss spectroscopy (EELS) log-ratio technique allowed to quantify the mean size and density of precipitates. Carbon extraction replicas were used to study the chemical composition of precipitates by energy dispersive X-ray spectrometry (EDS).

III. RESULTS

A. Initial Microstructure

The microstructure obtained in the cold-rolled state before annealing consists of martensite islands embedded in a ferrite matrix (Figure 1(a)). Phase fractions at this stage are similar for the five investigated grades with 70 pct \pm 5 pct ferrite and 30 pct \pm 5 pct martensite. Coarse TiN and (Ti,Nb)(C,N) precipitates formed

during hot-rolling can be observed at this stage (arrows in Figures 1(a) through (c)).

Fractions of precipitated Ti, Nb, and Mo in the cold-rolled sheets were determined (Figure 2). At this stage, only a small Mo fraction (25 mass ppm) has precipitated in Ref + Mo grade. About 25 pct of the nominal Nb content has already precipitated as (Ti,Nb)(C,N) in the cold-rolled sheet for all grades (Figure 2(a)). The strong affinity of titanium and nitrogen leads to extended precipitation of TiN particles, so that the precipitated titanium fraction in the hot-rolled sheet is mainly determined by the nitrogen content. For the studied grades, the nitrogen content is similar (40 or 50 mass ppm). It can thus be assumed that the amount of titanium which precipitated as TiN is similar for all the grades due to similar nitrogen contents, and that the amount of titanium which precipitated as (Ti,Nb)(C,N) increases with increasing the nominal content of titanium (Figure 2(b)). The important result for this study is that the trends defined for the nominal compositions are well preserved: the fraction of Nb which is still available in solid solution in the cold-rolled sheet is higher in Ref + Nb steel compared to the reference steel, and so on for the other grades (Figure 2).

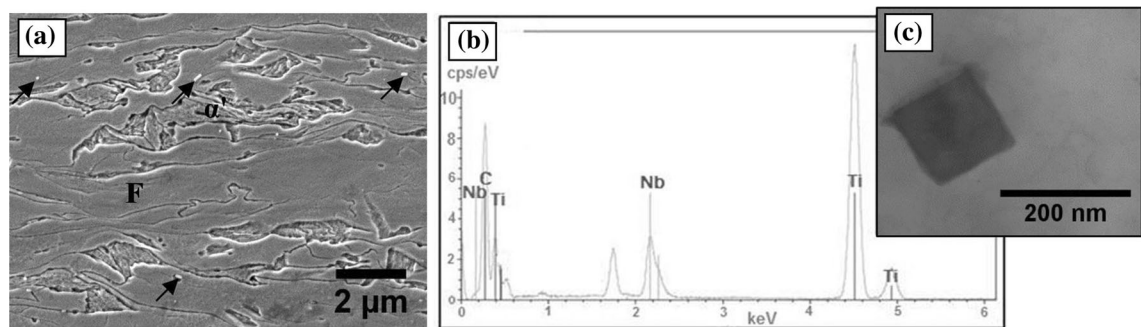


Fig. 1—(a) Ferrite(F)-martensite(α') cold-rolled microstructure (FEG-SEM, reference grade). Arrows indicate (Ti,Nb)(C,N) precipitates (b) EDS-spectrum of a coarse (Ti,Nb)(C,N) precipitate (carbon replica) and (c) the corresponding STEM-BF image.

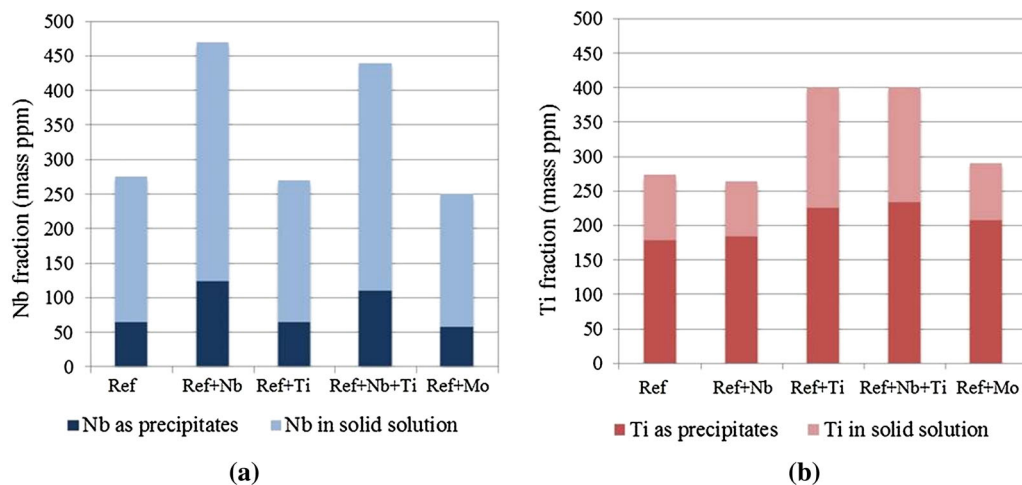


Fig. 2—Mass fractions of microalloying elements (a) Nb and (b) Ti precipitated as coarse TiN and (Ti,Nb)(C,N) in the cold-rolled sheets and still available in solid solution in the cold-rolled sheets.

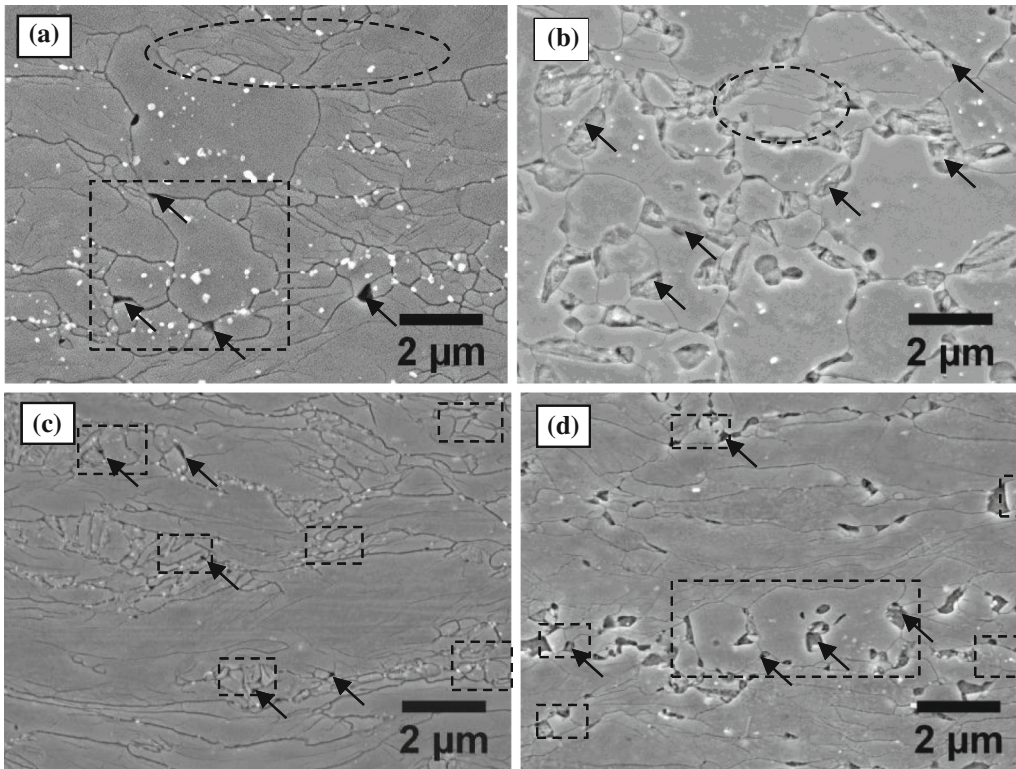


Fig. 3—Illustration of microstructural changes during heating at 1 K/s at (a) 983 K (710 °C) (b) 1023 K (750 °C) and at 10 K/s at (c) 983 K (710 °C) (d) 1023 K (750 °C) for Ref + Ti steel (FEG-SEM). Rectangles, ellipses, and arrows respectively indicate recrystallized ferrite, non-recrystallized ferrite, and austenite islands.

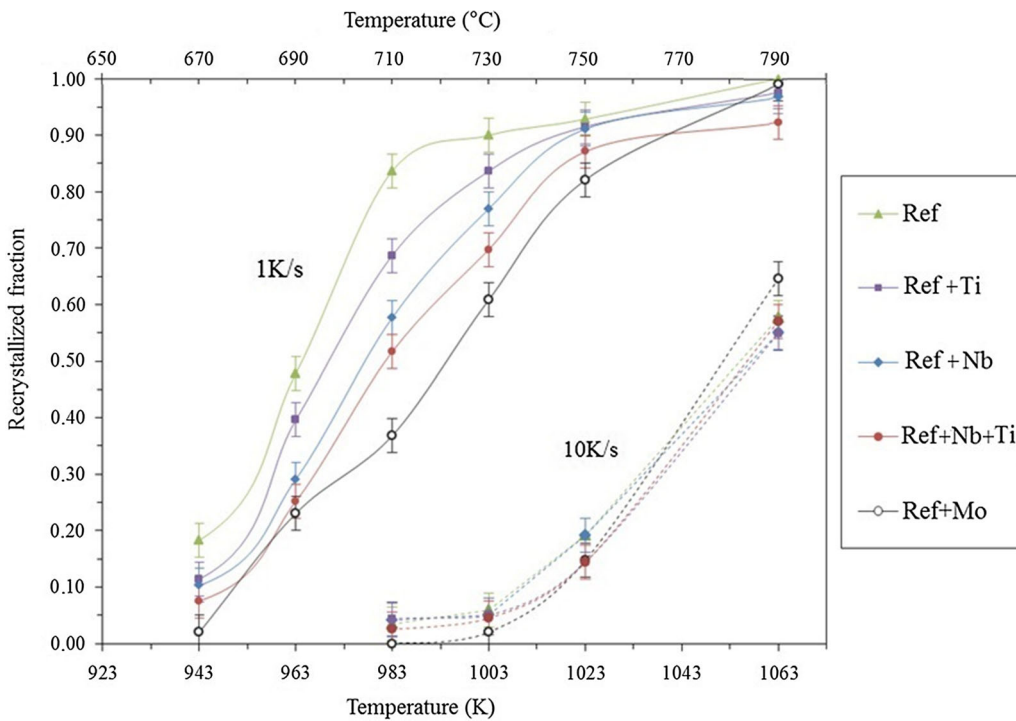


Fig. 4—Kinetics of recrystallization during continuous heating at 1 K/s (solid lines) and 10 K/s (dashed lines) for the five steel grades (recrystallization fraction is the ratio of recrystallized ferrite to total ferrite).

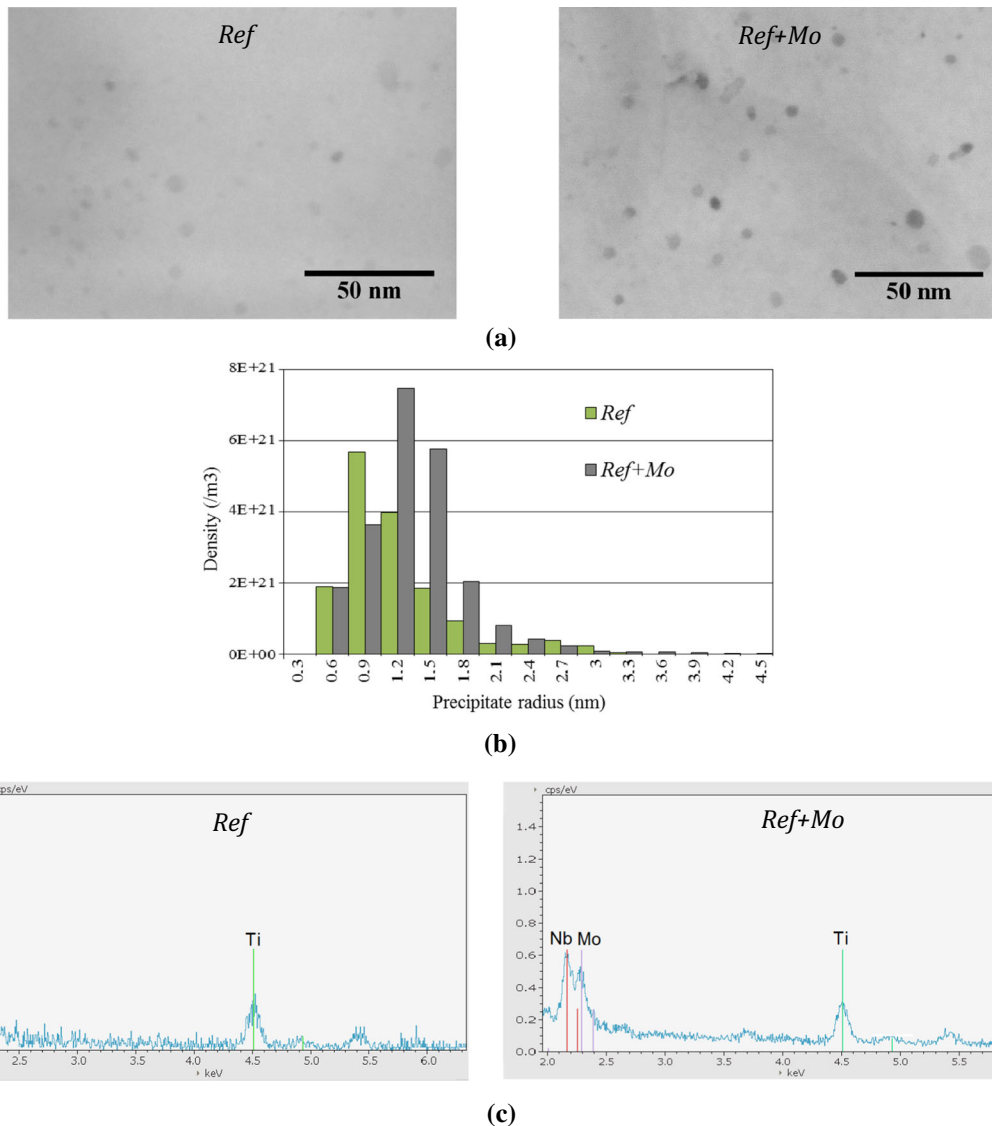


Fig. 5—Characterization of nano-scaled precipitates in Ref and Ref + Mo grades after heating at 1 K/s at 1023 K (750 °C): (a) observation of precipitates in recrystallized ferrite (STEM-BF, thin foil), (b) distribution of precipitates radii, (c) EDS-spectra of nano-scaled carbonitride precipitates (carbon replica).

B. Recrystallization Kinetics During Heating

Tempering of martensite islands occurs rapidly during heating from room temperature to 923 K (650 °C) and leads to the formation of cementite particles in prior martensite. Nucleation of recrystallization occurs in prior martensite islands or in their vicinity (dotted rectangles in Figures 3(a) and (c)) for the two heating rates. Micrographs after heating at 983 K (710 °C) (Figures 3(a) and (c)) show a major influence of heating rate on recrystallization: while recrystallization has already well progressed in the case of the low heating rate (Figure 3(a)), only a few recrystallized ferrite nuclei can be distinguished in the case of the high heating rate (Figure 3(c)). This also results in a different morphology of cementite particles (white dots in

Figures 3(a) and (c)), which are much larger and spheroidized in the case of slow heating. Nucleation sites for austenite (arrows in Figure 3) are identical for the two heating rates: regions with high cementite density situated in former martensite islands, which mostly correspond to recrystallized ferrite grain boundaries. However, both recrystallization of former martensite islands and cementite coarsening are not at the same stage of progress for the two heating rates. This leads to significantly different microstructures: large recrystallized ferrite and austenite grains homogeneously distributed in the microstructure for the slow heating rate (Figure 3(b)), small and dense recrystallized ferrite and austenite grains, both localized in the former martensite islands for the high heating rate (Figure 3(d)).

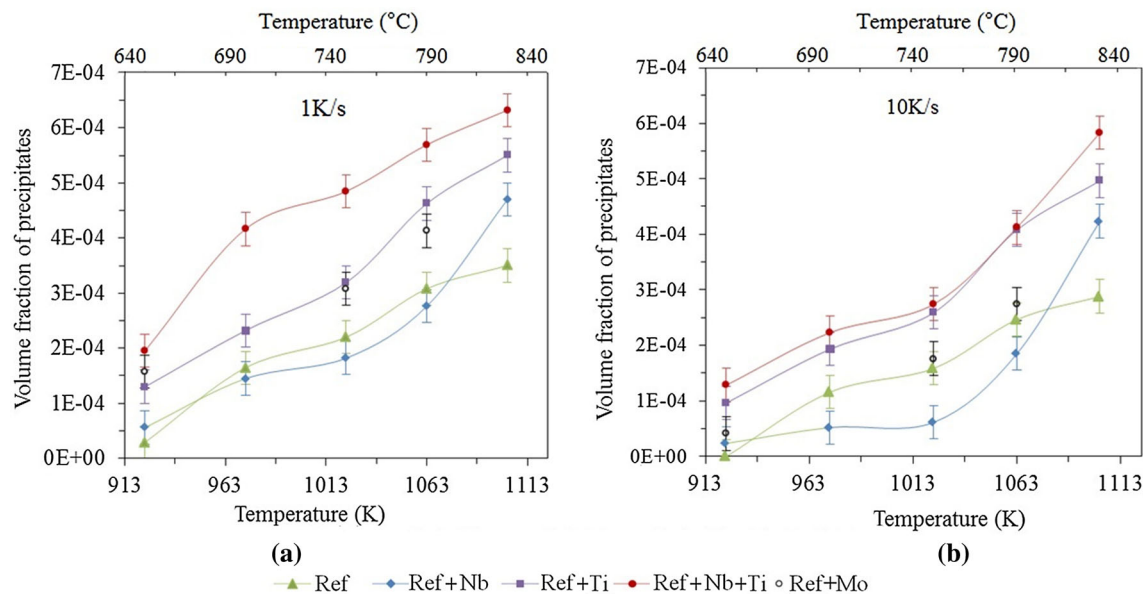


Fig. 6—Evolution of the volume fraction of (Ti,Nb)(C,N) or (Ti,Nb,Mo)(C,N) precipitates formed during continuous heating of the five steel grades at (a) 1 K/s, (b) 10 K/s.

Phase fractions were quantified by image analysis of these micrographs for the five steel grades and the two heating rates. Figure 4 represents the recrystallization fraction, calculated as the ratio of recrystallized ferrite to total ferrite. Recrystallization kinetics are strongly shifted towards higher temperatures when increasing the heating rate from 1 to 10 K/s for all the grades. The shift in temperature is between 60 K and 80 K. For the investigated chemical compositions and heating rates, the delaying effect due to increasing the heating rate from 1 to 10 K/s is stronger than the effect of microalloying elements addition: an effect of microalloying elements on delaying recrystallization can be seen in the case of the low heating rate but is not visible in the case of the high heating rate. Comparing recrystallization kinetics of the five grades for the low heating rate shows that recrystallization kinetics are shifted towards higher temperatures when increasing microalloying element content. The minimum shift in temperature is about 10 K and the maximum shift can reach 30 K. The comparative effect of Ti addition and Nb addition can be deduced by comparing results for Ref + Ti and Ref + Nb grades, for which the additional content of Ti or Nb compared to the reference grade is similar in terms of atomic fraction. The results show that the shift in temperature is larger when adding Nb than when adding Ti, indicating that Nb addition has a stronger delaying effect on recrystallization than Ti addition. Mo also has a strong influence on recrystallization kinetics, but its effect cannot be directly compared to Nb or Ti since Mo nominal content in the Ref + Mo steel is very high (900 mass ppm).

C. Precipitation Kinetics

STEM-BF observations on thin foils (Figure 5(a)) reveal the presence of fine carbonitride precipitation.

Figure 5(b) represents the distribution of precipitate radii obtained by image analysis and assuming spherical precipitates in Ref and Ref + Mo steels after heating at 1 K/s at 1023 K (750 °C). The presented distributions result from the analysis of around 500 precipitates located in various grains of a thin foil, corresponding to a minimum observed surface of $0.5 \mu\text{m}^2$. At this stage, the measured precipitate radii are in the range 0.3 to 4.5 nm. An example of EDS-spectra of such precipitates obtained on carbon extraction replica is shown in Figure 5(c) and confirms that they contain Nb and Ti in Ref grade, and Nb, Ti, and Mo in Ref + Mo grade. Reliable quantitative data regarding the chemical composition of these precipitates are however difficult to obtain using EDS analysis due to their small size.

The atomic fractions of precipitated Ti, Nb, and Mo obtained by matrix chemical dissolution were measured at different temperatures after heating at 1 or 10 K/s. The corresponding volume fraction of nano-scaled (Ti,Nb,Mo)(C,N) precipitates is calculated by adding the contribution of precipitated Ti, Nb, and Mo (assuming a molar volume of $12,83 \text{ cm}^3/\text{mol}$ for (Ti,Nb,Mo)(C,N)) and subtracting the contribution of precipitates already present in the initial cold-rolled stage (Figure 2). Results are represented in Figure 6.

Comparing the results obtained for the different grades first indicates that an addition of both Ti and Nb results in a higher volume fraction of (Ti,Nb)(C,N) precipitates (Figure 6, filled circles). Adding Ti alone has a similar effect (squares) but adding Nb alone does not increase the precipitate volume fraction (diamonds) until 1103 K (830 °C), indicating a different role of Ti and Nb for their co-precipitation as (Ti,Nb)(C,N). Mo addition also leads to a higher precipitate volume fraction (Figure 6, empty circles). For a given temperature, the volume fraction of precipitates is slightly lower when heating at 10 K/s than at 1 K/s.

IV. DISCUSSION

A. Effect of Heating Rate and Microalloying Elements on Recrystallization

The experimental study revealed a shift of the recrystallization kinetics towards higher temperatures when increasing the heating rate. This shift is certainly due to thermal effects, as reported in the literature^[5]: recrystallization progress is favored during slow heating because recrystallization is a thermally activated phenomenon and the time spent at each temperature increases with decreasing heating rate.

The experimental results indicate that increasing Ti, Nb, or Mo content delays the recrystallization kinetics when heating at 1 K/s. The shift in temperature obtained in case of increasing microalloying content is however not very large (30 K at most). The reason for this is probably that the reference steel grade Ref already contains some Ti and Nb. Investigating other steel grades without Ti and/or Nb would however be not particularly useful as far as the initial cold-rolled microstructure would inevitably be different.

Experimental results also showed that Nb addition is more efficient than Ti addition to delay recrystallization. When comparing the precipitation state and the recrystallization kinetics in Ref, Ref + Ti and Ref + Nb grades heated up at 1 K/s (see Figures 4 and 6(a)), it appears that the precipitation state in Ref and Ref + Nb is similar: sizes were estimated at 2.8 ± 0.2 nm in diameter for both grades at 1023 K (750 °C) for a heating rate of 1 K/s and volume fractions (see Figure 6(a)) are similar at least up to 1063 K

(790 °C)). However, recrystallization kinetics of Ref + Nb is delayed as compared to the Ref grade. This emphasizes that the major contribution in Ref + Nb grade for delaying recrystallization is due to Nb solute drag. Moreover, Ref + Ti has a higher volume fraction of precipitates [with a mean diameter of 3.0 ± 0.2 nm at 1023 K (750 °C)], whereas its recrystallization kinetics curve is only slightly shifted towards higher temperatures, as compared to the Ref grade. This suggests that precipitation effectiveness is lower than solute drag effect. This requires a deeper investigation of the comparative effectiveness of microalloying elements as solute and as precipitates on the one hand, and the comparative solute drag effect of the different microalloying elements (Ti, Nb, and Mo) on the other hand.

B. Modeling the Influence of Microalloying Elements and Heating Rate on Recrystallization

1. Modeling description

A simple modeling approach has been carried out to rationalize and clarify the influence of microalloying elements and heating rate on ferrite recrystallization. The influence of microalloying elements is introduced into the recrystallization model either as solute atoms by solute drag, acting on the mobility of the recrystallization front or as precipitates by Zener pinning, reducing the driving force for recrystallization. For such an approach, the volume fraction (f_v) and radius (R) of (Ti,Nb)(C,N) precipitates are required as well as the solute fraction remaining in solid solution ($X_{ss,i}$ with $i = \text{Nb, Ti, Mo}$). The separate fractions of precipitated

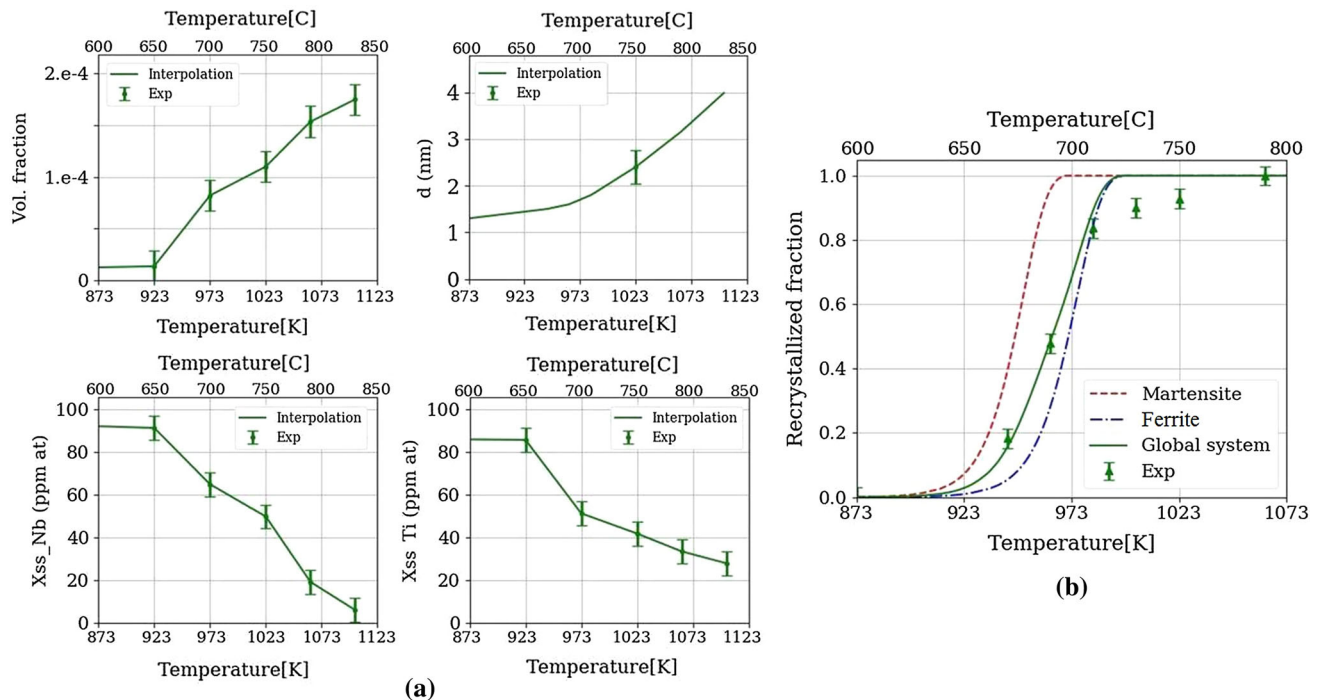


Fig. 7—Modeling results for Ref grade at 1 K/s between 873 K and 1073 K (600 °C and 800 °C). (a) Input data of the model based on interpolation of experimental data for the volume fraction of precipitates (f_v), the solute fraction remaining in solid solution ($X_{ss,Nb}$ and $X_{ss,Ti}$) and the evolution of the mean diameter of precipitates as calculated by a Deschamps–Bréchet-like model as compared to the experimental measurement at 1023 K (750 °C). (b) Recrystallized fraction calculated by the model and compared to experimental data points.

Ti, Nb, and Mo during heating were determined by matrix chemical dissolution at 923 K, 973 K, 1023 K, 1063, and 1103 K (650 °C, 700 °C, 750 °C, 790 °C, and 830 °C). The resulting volume fraction of precipitates was derived from these results (see Figure 6) together with the solute fraction remaining in solid solution calculated for each element as the difference between the fraction which is still available in solid solution in the cold-rolled sheet (see Figure 2) and the precipitated fraction. For calculations over the temperature range 873 K to 1073 K (600 to 800 °C), interpolation of experimental data was performed as illustrated in Figure 7(a) for the Ref grade. Concerning the precipitate mean radius, it was measured after heating at 1 K/s at 1023 K (750 °C) by image analysis on TEM micrographs (see Figure 5) for all grades and an estimation of its evolution during heating was derived from a classical precipitation model based on the Deschamps–Bréchet approach.^[23,24] Evolution of the mean radius as compared to the experimental point at 1023 K (750 °C) is displayed in Figure 7(a).

The recrystallization model relies on the approach developed by Zurob *et al.*^[25] based on Johnson–Mehl–Avrami–Kolmogorov (JMAK) theory. Recovery occurring at low temperatures, nor austenite formation are included in the model. Assuming site saturation, the expression of the extended recrystallized volume fraction is given by (Eq. [1]).

$$f_{\alpha_{\text{REX}}}^{\text{e}}(t) = N_{\text{REX}} \cdot \frac{4}{3} \pi \left(\int_0^t M_{\text{REX}}(t) E_{\text{REX}}(t) dt \right)^3, \quad [1]$$

where N_{REX} is the number of nucleation sites for recrystallization per unit volume; E_{REX} is the driving force for recrystallization, and M_{REX} is the mobility of the recrystallization front. The mobility is reduced by the solute drag effect of microalloying elements which is expressed using Eq. [2].

$$M_{\text{REX}}(t) = \frac{M_{\text{pure}}}{1 + \sum_i \alpha_i X_{\text{ss},i}}, \quad [2]$$

with $i = \text{Nb, Ti, Mo}$.

M_{pure} is the intrinsic grain boundary mobility, which is temperature dependent (Eq. [3]), and α_i is a constant representative of the amplitude of the solute drag effect due to element i .

$$M_{\text{pure}} = \frac{D_{\text{gb}}^0 V_{\text{Fe}}}{R_{\text{gp}} T \lambda} \exp\left(-\frac{Q_{\text{gb}}}{R_{\text{gp}} T}\right), \quad [3]$$

D_{gb}^0 and Q_{gb} are respectively the pre-exponential factor and activation energy for grain boundary mobility; V_{Fe} is ferrite molar volume (7.11 cm³/mol) and λ is the grain boundary thickness (0.25 nm).

The driving force for recrystallization corresponds to the stored energy of deformation reduced by the Zener pinning effect due to precipitates (Eq. [4]).

$$E_{\text{REX}}(t) = E_{\text{REX},0} - \frac{3}{2} \gamma_{\text{gb}} \frac{f_v}{R} = \frac{1}{2} \mu b^2 \rho - \frac{3}{2} \gamma_{\text{gb}} \frac{f_v}{R}. \quad [4]$$

The stored energy of deformation $E_{\text{REX},0}$ is expressed as a function of the dislocation density ρ , the shear modulus μ , and the Burgers vector b . γ_{gb} is the interfacial energy of the grain boundary.

In order to take into account the initial bi-phased cold-rolled microstructure, the modeled system is separated into two sub-systems modeling the initial ferrite and martensite phases. The initial martensite and ferrite regions are assumed to differ in their dislocation density, assumed to be higher in martensite. The behavior of the global system is derived by a summation of each sub-system weighted by the volume fraction of the corresponding phase in the initial state (70 pct ferrite and 30 pct martensite).

The values of the key parameters used in the model (Table II) were defined to fit into the range of experimental or modeling values given in the literature and were then adjusted by comparison to the experimental data. Modeling results for recrystallization of Ref grade at 1 K/s are represented in Figure 7(b). Such a model is able to reproduce the effect of microalloying elements on recrystallization observed experimentally.

Table II. Values of the Key Parameters Used in the Recrystallization Model

Parameter	Symbol	Unit	Values Reported in the Literature	Value Used in the Model
Dislocation Density	ρ	m ⁻²	5.2×10^{14} ^[26]	$\rho_{\text{ferrite}} = 5 \times 10^{14}$ $\rho_{\text{martensite}} = 1 \times 10^{15}$
Grain Boundary Energy	γ_{gb}	J m ⁻²	0.5 ^[21] 0.75 ^[27]	1.0
Number Density of Recrystallization Nucleation Sites	N_{REX}	m ⁻³	5×10^{14} ^[26] 1.5×10^{15} ^[28]	2×10^{15}
Prefactor for Grain Boundary Mobility	D_{gb}^0	m ² s ⁻¹	1.5×10^{-4} ^[26]	0.01
Activation Energy for Grain Boundary Mobility	Q_{gb}	J mol ⁻¹	148,000 ^[26] 253,000 ^[27] 180,000 ^[28] 226,000 ^[29]	210,000

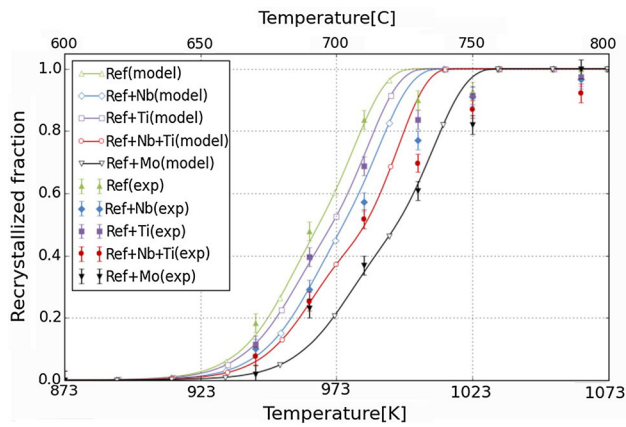


Fig. 8—Modeled evolution of the recrystallized fraction during heating at 1 K/s for the five investigated grades, with $\alpha_{Ti} < \alpha_{Mo} < \alpha_{Nb}$.

2. Comparing solute drag of Nb, Ti, and Mo and precipitate pinning effects

In order to go deeper into the understanding of the separate effect of microalloying elements, the described recrystallization model was applied to the five investigated grades. Modeling results for heating at 1 K/s are displayed in Figure 8.

Satisfying agreement with experimental results is found for $\alpha_{Nb} = 6.5 \times 10^3$, $\alpha_{Mo} = 3 \times 10^3$, and $\alpha_{Ti} = 6 \times 10^2$, showing that the order of effectiveness of microalloying elements in retarding recrystallization by solute drag is Nb > Mo > Ti. The strength of solute drag effect is higher for solute Nb than for solute Mo and Ti. This difference might be due to a disparity in atomic radius or electronic structure between Fe and solute atoms.

Figure 9 shows the separate contribution of Zener pinning and solute drag on shifting recrystallization towards higher temperatures for the four Ti and

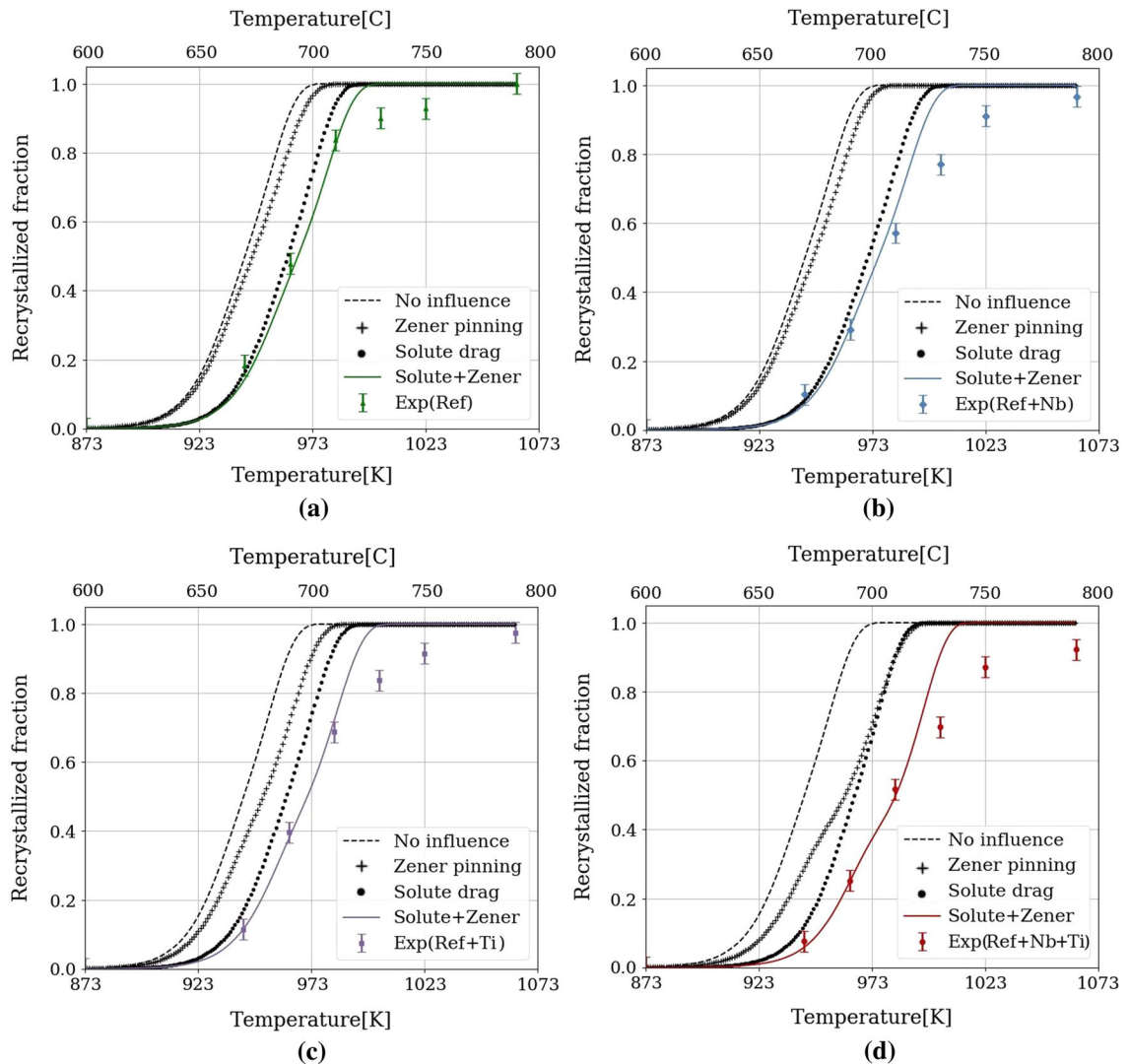


Fig. 9—Modeled contribution of solute drag and precipitate pinning for (a) Ref, (b) Ref + Nb, (c) Ref + Ti, and (d) Ref + Nb + Ti grades.

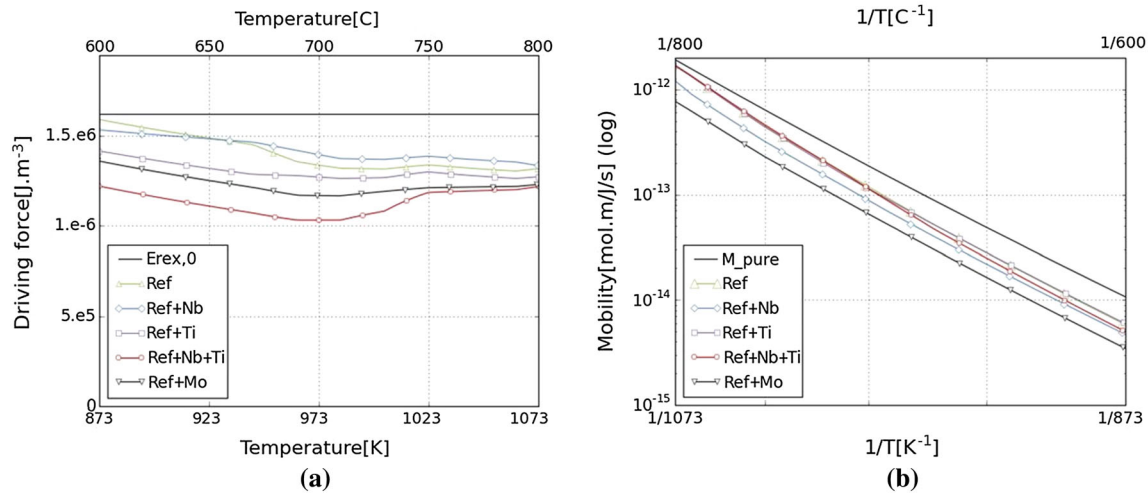


Fig. 10—Modeled evolution of (a) the driving force for recrystallization and (b) the mobility of recrystallization front during heating at 1 K/s for the five investigated grades, with $\alpha_{Ti} < \alpha_{Mo} < \alpha_{Nb}$.

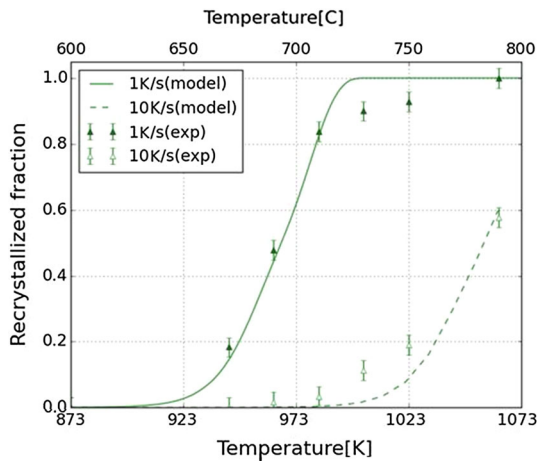


Fig. 11—Modeled recrystallization kinetics for Ref grade during heating at 1 and 10 K/s.

Nb-bearing grades, indicating that the predominant effect delaying recrystallization is solute drag. The overall delay in recrystallization in Ref and Ref + Nb grades is almost only due to solute drag, whereas it is due to a combination of solute drag and precipitate pinning effects in Ref + Ti and Ref + Nb + Ti grades. These results also show that the delay in recrystallization kinetics between Ref and Ref + Nb + Ti grades does not originate from a larger solute drag effect in Ref + Nb + Ti grade, but from an increased Zener pinning effect due to a modified precipitation state coming from the additional Ti and Nb nominal content.

At this point, the global effect of microalloying elements addition can be further understood by comparing the effect of precipitates on the recrystallization driving force and the effect of solute elements on the mobility of the recrystallization front in the different grades (Figure 10). These modeling results show that

$$\begin{aligned}
 E_{\text{REX}}(\text{Ref}) &\sim E_{\text{REX}}(\text{Ref} + \text{Nb}) > E_{\text{REX}}(\text{Ref} + \text{Ti}) \\
 &> E_{\text{REX}}(\text{Ref} + \text{Mo}) > E_{\text{REX}}(\text{Ref} + \text{Nb} + \text{Ti})
 \end{aligned}
 \tag{5}$$

and

$$\begin{aligned}
 M_{\text{REX}}(\text{Ref}) &\sim M_{\text{REX}}(\text{Ref} + \text{Ti}) \\
 &\sim M_{\text{REX}}(\text{Ref} + \text{Nb} + \text{Ti}) \\
 &> M_{\text{REX}}(\text{Ref} + \text{Nb}) > M_{\text{REX}}(\text{Ref} + \text{Mo}).
 \end{aligned}
 \tag{6}$$

Adding Nb alone significantly reduces the mobility because of the high amount of Nb in solid solution and the strong solute drag effect of Nb, while adding Ti alone reduces the driving force because of the modified precipitation state. The increased volume fraction of precipitates due to Ti addition reduces the driving force. The decrease in mobility due to Nb addition leads to a stronger impeding effect on recrystallization than the decrease in driving force due to Ti addition (Figure 10). Adding both Ti and Nb results in an extended carbonitride precipitation and thus leads to a significant reduction of the driving force but has little effect on the mobility. Adding Mo reduces both the mobility and the driving force due to a high amount of Mo in solid solution together with an extended carbonitride precipitation during heating.

3. Effect of heating rate

The recrystallization model was applied for the 2 heating rates using the same parameters (Table II). Modeling results (Figure 11) reproduce the shift of the recrystallization mechanism towards higher temperatures when increasing the heating rate and thus confirms that it is due to thermal effects. However, the fit to experimental results when increasing the heating rate is not perfect. A reason for this might be that a lower degree in recovery occurs for the high heating rate before

recrystallization starts, leading to a higher dislocation density and then to a higher driving force for further recrystallization. As a consequence, the model underestimates the recrystallization kinetics at 10 K/s.

V. SUMMARY

The present work investigates the effects of heating rate and microalloying elements Ti, Nb, and Mo on ferrite recrystallization during annealing of Dual-Phase steels. Experimental study of different steel grades having the same ferrite-martensite cold-rolled microstructure revealed that ferrite recrystallization is shifted towards higher temperatures when increasing the heating rate or microalloying element content. For the investigated chemical compositions and heating rates, the delay in recrystallization due to increasing the heating rate from 1 to 10 K/s is stronger than the effect of microalloying elements addition.

Coupling the experimental results with modeling allows clarification regarding the effect of microalloying elements on recrystallization. Using reasonable values for the key parameters, our model shows that, in the present case, a large contribution in recrystallization is due to solute drag, in particular in Nb-bearing grades, and that the different elements do not have the same solute drag retardation effect: Nb has the highest solute drag effect, followed by Mo and finally Ti.

ACKNOWLEDGMENTS

This project was supported by the National Association of Research and Technology (ANRT – Project no. 615/2014). The authors are grateful to Patrick Barges from the Automotive Product Center – ArcelorMittal R&D for his help with the TEM analysis.

REFERENCES

1. N. Pottore, N. Fonstein, I. Gupta, D. Bhattacharya: Proceedings of the International Conference on Advanced High Strength Sheet Steels for Automotive Applications, 2004, pp. 119–30.

2. D.K. Matlock, G. Krauss, and J.G. Speer: *Mater. Sci. Forum*, 2005, vols. 500–501, pp. 87–96.
3. W. Bleck and K. Phiu-on: *Microstructure and Texture in Steels*, Springer, London, 2009, pp. 145–63.
4. O. Bouaziz, H. Zurob, and M. Huang: *Steel Res. Int.*, 2013, vol. 84, pp. 937–47.
5. F.J. Humphreys and M. Hatherly: *Recrystallization and Related Annealing phenomena*, Elsevier Science Ltd., Oxford, 1995.
6. J. Huang, W.J. Poole, and M. Militzer: *Metall. Mater. Trans. A*, 2004, vol. 35A, pp. 3363–75.
7. A. Chbihi, D. Barbier, L. Germain, A. Hazotte, and M. Goune: *J. Mater. Sci.*, 2014, vol. 49, pp. 3608–21.
8. C. Philippot, J. Drillet, P. Maugis, V. Hebert, and M. Dumont: *Metall. Res. Technol.*, 2014, vol. 111, pp. 3–8.
9. D. Muljono, M. Ferry, and D.P. Dunne: *Mater. Sci. Eng. A*, 2001, vol. 303, pp. 90–99.
10. S. Vervynck, K. Verbeken, P. Thibaux, and Y. Houbaert: *Mater. Sci. Eng. A*, 2011, vol. 528, pp. 5519–28.
11. M. Gomez, A. Quispe, and S.F. Medina: *Steel Res. Int.*, 2014, vol. 85, pp. 1440–45.
12. H.L. Andrade, M.G. Akben, and J.J. Jonas: *Metall. Mater. Trans. A*, 1983, vol. 14A, pp. 1967–77.
13. R. Song, N. Fonstein, H.J. Jun, N. Pottore, D. Bhattacharya, and S. Jansto: *Metallogr. Microstruct. Anal.*, 2014, vol. 3, pp. 174–84.
14. C. Capdevila, T. De Cock, C. Garcia-Mateo, F.G. Caballero, and C. Garcia de Andres: *Mater. Sci. Forum*, 2005, vols. 500–501, pp. 803–10.
15. J.W. Cahn: *Acta Metall.*, 1962, vol. 10, pp. 789–98.
16. M. Hillert and B. Sundman: *Acta Metall.*, 1976, vol. 24, pp. 731–43.
17. C.S. Smith: *Trans. Metall. Soc. AIME*, 1948, vol. 175, pp. 15–51.
18. J.G. Speer and S.S. Hansen: *Metall. Mater. Trans. A*, 1989, vol. 20A, pp. 25–38.
19. B. Pereda, A.I. Fernandez, B. Lopez, and J.M. Rodriguez-Ibabe: *ISIJ Int.*, 2007, vol. 47, pp. 860–68.
20. M.G. Akben, I. Weiss, and J.J. Jonas: *Acta Metall.*, 1981, vol. 29, pp. 111–21.
21. C. Hutchinson, H. Zurob, C. Sinclair, and Y. Brechet: *Scripta Mater.*, 2008, vol. 59, pp. 635–37.
22. S.F. Medina and C.A. Hernandez: *Acta Mater.*, 1996, vol. 44, pp. 165–71.
23. A. Deschamps and Y. Brechet: *Acta Mater.*, 1998, vol. 47, pp. 293–305.
24. M. Gouné, P. Maugis, and F. Danoix: *Nanotechnology Reviews.*, 2015, vol. 4, pp. 517–32.
25. H.S. Zurob, C.R. Hutchinson, Y. Brechet, and G. Purdy: *Acta Mater.*, 2002, vol. 50, pp. 3077–94.
26. C. Sinclair, C.R. Hutchinson, and Y. Brechet: *Metall. Mater. Trans. A*, 2007, vol. 38A, pp. 821–30.
27. H.S. Zurob, Y. Brechet, and G. Purdy: *Acta Mater.*, 2001, vol. 49, pp. 4183–90.
28. C. Bos, M.G. Meozzi, and J. Sietsma: *Comput. Mat. Sci.*, 2010, vol. 48, pp. 692–99.
29. D.Z. Yang, E.L. Brown, D.K. Matlock, and G. Krauss: *Metall. Mater. Trans. A*, 1985, vol. 16A, pp. 1385–92.